Numerical Analysis of an Impact on an Aircraft's Fuselage

Nikolaos Monogyios*, Will Brizzolara†, Gabriel Esquivel‡, and Ka'inoa Lugo§
University of Illinois Urbana-Champaign

In this report, we applied numerical method principles to solve an IBVP. The topic chosen to model is applying a distributed impact force on an aircraft's fuselage. A governing equation will be defined to create a mathematical representation of the problem. The trapezoidal method will be used to solve this problem due to its high stability and accuracy, energy conservation, and efficiency for long simulations. Python will be used to run the numerical method and simulations using the IBVP. Finally, plots and data are presented to explain the results of the numerical approach and answer any guiding questions for the problem.

I. Nomenclature

$w(x, y, t)$	=	Transverse displacement (m)
$\rho h \dfrac{\partial^2 w}{\partial t^2}$	=	Inertial force per unit area (N/m^2)
ρh	=	Mass per unit area (kg/m^2)
$K_0 w$	=	Linear foundation restoring force per unit area (N/m^2)
K_0	=	Elastic foundation stiffness per unit area (N/m^3)
$T\nabla^2 w$	=	Membrane tension contribution (N/m^2)
T	=	In-plane tension per unit length (N/m)
$D\nabla^4 w$	=	Kirchhoff–Love bending term (N/m^2)
D	=	Flexural rigidity (N·m)
$K_1 \dfrac{\partial w}{\partial t}$	=	Viscous damping force per unit area (N/m^2)
K_1	=	Viscous damping coefficient per unit area (N·s/m^3)
$F(\mathbf{x}, t)$	=	External forcing per unit area (N/m^2)
H	=	Height of the plate (mm)
$\mathbf{x} = (x, y)$	=	In-plane coordinates on the plate (m)
t	=	Time (s)
n	=	Number of intervals in each spatial direction
h	=	Grid spacing in x and y (m)
i, j	=	Grid indices in the x- and y-directions, $i, j = 1, \ldots, n+1$
k	=	Index for interior nodes, $k = 0, \ldots, (n-1)^2 - 1$
$w_{i,j}$	=	Discrete transverse displacement at grid point (i, j) (m)
$\partial\Omega$	=	Plate boundary
M	=	Mass matrix (kg/m^3)
C	=	Damping matrix (N)
K	=	Stiffness matrix (N/m^3)
L_2	=	Laplacian Matrix
L_4	=	Biharmonic Matrix
τ_k	=	Truncation error
$R(z)$	=	Amplification factor of trapezoidal method
$w(t)$	=	Vector representing the out of plate nodal displacements
$f(t)$	=	External forces vector
$\ddot{w}_{k+1}$	=	Acceleration vector at t_{k+1}

*Undergraduate Student, Aerospace Engineering, Talbot Laboratory, 104 S Wright St, Urbana, IL 61801
†Undergraduate Student, Aerospace Engineering, Talbot Laboratory, 104 S Wright St, Urbana, IL 61801
‡Undergraduate Student, Aerospace Engineering, Talbot Laboratory, 104 S Wright St, Urbana, IL 61801
§Undergraduate Student, Aerospace Engineering, Talbot Laboratory, 104 S Wright St, Urbana, IL 61801

$F(x, y, t)$	=	Distributed transverse load (pressure) (N/m^2)
F_0	=	Peak load amplitude (N/m^2)
a	=	Time at which the load reaches its maximum (s)
b	=	Time where force has maximum magnitude (s)

II. Introduction to the IBVP

A. Background information and motivation for the chosen IBVP

Numeral methods in engineering are used to obtain approximate solutions to complex systems that cannot be solved analytically. One example of applying numerical methods is to solve an Initial Boundary Value Problem (IBVP). It is a type of PDE in space and time that consists of initial conditions (IC) in time (t = 0) and boundary conditions (BC) in space. For this project, we will use an IBVP to model the plate response to a distributed force. Specifically, we are measuring a distributed impact force on an aircraft's fuselage. The topic will be modeled using a governing equation with I.Cs and B.Cs defined.

The chosen concept is important in a real-world scenario as Engineers use distributed forces to test the safety, design, performance, and durability of an aircraft. One case that represents this is the distributed loading conditions that an aircraft experiences during an emergency landing [1]. An emergency landing is a type of complex, nonlinear, distributed event where the aircraft experiences large deformation, material fracture, structural failure, and dynamic contact. These forces are distributed among the fuselage during impact. Engineers analyse this type of distributed damage to reduce catastrophic structural failure and significant casualties in future events. Another case that represents the chosen topic is analysing the distributed forces from debris. One type of debris impact is tire fragments from an aircraft's tire bursting and striking the fuselage [2]. Even though the fragment striking the fuselage can be considered an impact force, distributed forces are at play due to the force being transmitted through a finite contact area. This is known as pressure distributed over a surface, which is the fuselage in this case. Engineers analyse this type of distributed forcing to compare different structural/material resistance.

B. Defining the Governing Equation for the IBVP

To model the chosen concept, we will refer to a governing equation that applies Kirchhoff-Love plate theory for linear, elastic, and small-deflections on a thin plate [3]. It is assumed that the plate is isotropic, homogeneous, and thin with thickness h. Three different materials, aluminum, stainless steel, and titanium, will be used to test the IBVP. It will also be assumed that the normals remain straight and perpendicular, and the thickness of the plate remains the same during deformation. The governing equation is defined as:

$$\rho h \frac{\partial^2 w}{\partial t^2} = -K_0 w + T\nabla^2 w - D\nabla^4 w - K_1 \frac{\partial w}{\partial t} + F(\mathbf{x}, t) \tag{1}$$

Eq. (1) is a linear, second-order-in-time, fourth-order-in-space PDE. On the left handed side, $\rho h \frac{\partial^2 w}{\partial t^2}$ is the inertial force per unit area. This expression measures the resistance to changes in motion, where increasing ρh increases inertia. On the right-hand side, $K_0 w$ is the linear foundation stiffness. This expression represents the distributed force as a spring that pulls the plate back toward $w = 0$. If the elastic stiffness K_0 is larger, then the plate is more likely to stay flat. $T\nabla^2 w$ represents the membrane/tension effect. It states that if the plate is stretched, curvature in $w(x, y, t)$ produces an additional restoring force. $D\nabla^4 w$ represents the Kirchhoff–Love bending term. It penalizes curvature and gives the plate its resistance to bending. $K_1 \frac{\partial w}{\partial t}$ is the viscous damping term, which shows the effect of removing energy from the system and shows vibration decay. Finally, $F(\mathbf{x}, t)$ is the external forcing term that represents the distributed force on the surface in terms of x, y, t. The spatial operators for the governing equation are defined as:

$$\nabla^2 w = \frac{\partial^2 w}{\partial x^2} + \frac{\partial^2 w}{\partial y^2} \quad \text{(Laplacian)} \tag{2}$$

$$\nabla^4 w = \frac{\partial^4 w}{\partial x^4} + 2\frac{\partial^4 w}{\partial x^2 \partial y^2} + \frac{\partial^4 w}{\partial y^4} \quad \text{(Biharmonic)} \tag{3}$$

For Eq. (1) to be defined as an IBVP, initial conditions (I.Cs) and boundary conditions (B.Cs) must be specified in time and space, respectively. The plate is assumed to be clamped (built-in). Using this condition, the boundary is

restrained along the plate boundary $\partial\Omega$, which gives us two B.Cs. They are defined as $w = 0$ and $\dfrac{\partial w}{\partial n} = 0$ for $x \in \partial\Omega$, where $w = 0$ is the transverse displacement at the edge and $\partial/\partial n = 0$ shows there is zero slope/rotation at the midedge. Proper I.Cs to align with the B.Cs are defined as $w(x, 0) = w_0(x) = 0$ and $\dfrac{\partial w}{\partial t}(x, 0) = v_0(x) = 0$, set at $t = 0$. The I.Cs. tell us that at $t = 0$, the plate is initially flat (undeformed) and at rest. All motion afterwards is caused only by the forcing term $F(\mathbf{x}, t)$

From the governing equation, $F(\mathbf{x}, t)$ was defined as the external forcing term representing the distributed force on the plate. To measure the distributed forcing on the plate, $F(\mathbf{x}, t)$ will be set as:

$$F(x, y, t) = F_0 \exp\left(-\frac{(t-a)^2}{2b^2}\right) \sin\left(\frac{\pi x}{l} - \frac{\pi}{2}\right) \sin\left(\frac{\pi y}{l} - \frac{\pi}{2}\right), \tag{4}$$

F_0 is the overall load amplitude. The expression $\exp\left(-(t-a)^2/(2b^2)\right)$ represents the Gaussian factor which provides a smooth, impact-like pulse in time. The load peaks at time a, which is when the force reaches its absolute maximum, and b is the time at which the force has a maximum magnitude of 0.3% that of F_0. $F(\mathbf{x}, \mathbf{y}, t)$ is a continuous distributed load field on the plate applied at all points.

C. Parameters and Guiding questions for the IBVP

Table (2) defines the parameters used for the IBVP. The plate will have dimensions of 0.5 x 0.5 m, with a height of $H = 2mm$. Three different materials, aluminum, stainless steel, and titanium, are used to test the IBVP. This is done to test and analyze how different material properties react differently to the distributed force being applied on the plate. It is noted that $T = 0$ in table (2) because we assume that the plates are not pretensioned before the force of the impact is applied to them. In the numerical solution provided for this report, the Laplacian term was considered as if T was not zero in order to create a general solution that can be applied to problems where the plates are pretensioned. An example of this case would be a plate of the fuselage of the plane cruising at high altitude, where the difference in pressure between the inside and outside creates tension in the panel.

Table 2 Coefficients Appearing in the Kirchhoff–Love Plate Equation (0.5×0.5 **m,** $H = 2$ **mm, CCCC)**

Material	E (GPa)	ν	ρ (kg/m^3)	ρh (kg/m^2)	D (N·m)	T (N/m)	K_0 (N/m)	K_1 (N·s/m)
Aluminum (6061-T6)	68.9	0.33	2700	5.40	51.6	0	5.27×10^4	2.77
Stainless Steel (304)	193	0.29	8000	16.0	143	0	2.54×10^5	5.24
Titanium (Ti-6Al-4V)	113.8	0.34	4430	8.86	84.8	0	1.09×10^5	10.2

To guide us in modeling the IBVP with our model, we will reference the following questions:
1) How does the stress field $\sigma(x, y, t)$ vary across the plate over time?
2) What is the maximum stress in the plate, and where and when does it occur?
3) How does the plate vibrate after impact (deflection vs. time at key points)?
4) How do different materials (aluminum, stainless steel, titanium) respond to impacts?

III. Numerical Approach for the IBVP

This section describes the numerical procedure used to solve the IBVP governing the behavior of a thin rectangular plate. The governing PDE is first discretized in space using finite difference methods, giving us a system of ODEs in time. This system is then integrated in time using the Trapezoidal Method.

A. Spatial Discretization of the Governing Equation

1. Grid Setup

The rectangular plate chosen for the problem is discretion on a uniform $(n + 1) \times (n + 1)$ grid, with grid indices $i, j = 1, 2, \ldots, n + 1$ and grid spacing h in both the x- and y-directions, resulting in a total of $(n + 1)^2$ grid points. The boundary of the plate corresponds to the grid lines $i = 1$, $i = n + 1$, $j = 1$, and $j = n + 1$, where the clamped boundary condition enforces $w = 0$. The interior nodes, at which the PDE is solved, are those with indices $i, j \in \{2, 3, \ldots, n\}$, giving a total of $(n - 1)^2$ interior points. The 2D grid indices(i, j) is mapped to a single 1D index k:

$$k = (i-2) + (n-1)(j-2), \quad i, j \in \{2, 3, \ldots, n\}, \tag{5}$$

where $k = 0, 1, ..., (n-1)^2 - 1$ runs from 0 to $(n-1)^2 - 1$. The solution vector is then defined as:

$$\mathbf{w} = (w_{2,2},\, w_{3,2},\, \ldots,\, w_{n,2},\, w_{2,3},\, \ldots,\, w_{n,n})^T. \tag{6}$$

The inverse mapping, which recovers the pair (i, j) from a given k, is:

$$i = (k \bmod (n-1)) + 2, \qquad j = \left\lfloor \frac{k}{n-1} \right\rfloor + 2 \tag{7}$$

so that each entry of $\mathbf{w}$ is associated with a unique grid point (i, j) in the two-dimensional domain.

2. Initial and Boundary Conditions

Note that while the boundary and initial conditions were defined in continuous form in the IBVP introduction, their numerical form on the discrete grid is described here. For Eq. (1) to be defined as an IBVP, initial conditions (I.Cs) and boundary conditions (B.Cs) must be specified in time and space, respectively. The I.Cs $w(\mathbf{x}, 0) = 0$ and $w_t(\mathbf{x}, 0) = 0$ are selected to represent a plate that starts flat and motionless at $t = 0$. At this time, there is no displacement or velocity. Since the plate is assumed to be clamped to the fuselage, clamped B.Cs are imposed along the plate boundary $\partial\Omega$ to model attachment to the fuselage. These B.Cs are $w = 0$ and $\partial w/\partial n = 0$, which represent zero transverse displacement and zero rotation/normal slope on $\partial\Omega$ respectively.

On the $(n+1) \times (n+1)$ grid, clamped boundary conditions are enforced by two conditions: zero transverse displacement and zero normal derivative boundary. The zero-displacement condition is applied directly at all boundary nodes, so that $w_{1,j} = w_{n+1,j} = w_{i,1} = w_{i,n+1} = 0$. The zero normal-derivative condition, $\partial w/\partial \mathbf{n}|_{\text{boundary}} = 0$, is implemented using a second-order approximation, which introduces ghost points outside the computational domain. For the left boundary ($i = 1$), the approximation $\partial w/\partial x|_{1,j} \approx (w_{2,j} - w_{0,j})/(2h) = 0$ yields $w_{0,j} = w_{2,j}$. Applying the same approach on the remaining boundary gives $w_{n+2,j} = w_{n,j}$ at the right boundary ($i = n+1$), $w_{i,0} = w_{i,2}$ at the bottom boundary ($j = 1$), and $w_{i,n+2} = w_{i,n}$ at the top boundary ($j = n+1$). Table (3) shows a summary of all ghost points on each boundary.

Boundary	Ghost Point	Mirrors To	*Relation*
Left ($i = 1$)	$w_{0,j}$	$w_{2,j}$	$w_{0,j} = w_{2,j}$
Right ($i = n+1$)	$w_{n+2,j}$	$w_{n,j}$	$w_{n+2,j} = w_{n,j}$
Bottom ($j = 1$)	$w_{i,0}$	$w_{i,2}$	$w_{i,0} = w_{i,2}$
Top ($j = n+1$)	$w_{i,n+2}$	$w_{i,n}$	$w_{i,n+2} = w_{i,n}$

Table 3 Ghost Points derived from the conditions.

3. Discretization of the Laplacian

The Laplacian operator $\nabla^2 w = \frac{\partial^2 w}{\partial x^2} + \frac{\partial^2 w}{\partial y^2}$ is approximated on a uniform grid using second-order finite differences. At the grid indices (i, j) with spacing h in both directions, the second derivatives are discretized as:

$$\left.\frac{\partial^2 w}{\partial x^2}\right|_{i,j} \approx \frac{w_{i+1,j} - 2w_{i,j} + w_{i-1,j}}{h^2}, \tag{8}$$

$$\left.\frac{\partial^2 w}{\partial y^2}\right|_{i,j} \approx \frac{w_{i,j+1} - 2w_{i,j} + w_{i,j-1}}{h^2}. \tag{9}$$

Adding these two approximations yields the Discrete Laplacian (five-point stencil):

$$\nabla^2 w\big|_{i,j} \approx \frac{1}{h^2}\left(w_{i+1,j} + w_{i-1,j} + w_{i,j+1} + w_{i,j-1} - 4w_{i,j}\right) \tag{10}$$

The stencil can be written in matrix form as:

$$\nabla^2 \approx \frac{1}{h^2}\begin{pmatrix} & 1 & \\ 1 & -4 & 1 \\ & 1 & \end{pmatrix}. \tag{11}$$

The center coefficient multiplies $w_{i,j}$ and the surrounding coefficients multiply the neighboring grid values.

4. Discretization of the Biharmonic

The same process for discretizing the Laplacian operator is repeated for the Biharmonic operator. The biharmonic operator $\nabla^4 w = \frac{\partial^4 w}{\partial x^4} + 2\frac{\partial^4 w}{\partial x^2 \partial y^2} + \frac{\partial^4 w}{\partial y^4}$ is discretized using second-order finite differences on a uniform grid with spacing h. At the grid indices (i, j), the pure fourth derivative in the x-direction is approximated by the five-point stencil:

$$\left.\frac{\partial^4 w}{\partial x^4}\right|_{i,j} \approx \frac{w_{i+2,j} - 4w_{i+1,j} + 6w_{i,j} - 4w_{i-1,j} + w_{i-2,j}}{h^4}. \tag{12}$$

The process is repeated for approximating the pure fourth derivative in the y-direction:

$$\left.\frac{\partial^4 w}{\partial y^4}\right|_{i,j} \approx \frac{w_{i,j+2} - 4w_{i,j+1} + 6w_{i,j} - 4w_{i,j-1} + w_{i,j-2}}{h^4}. \tag{13}$$

The mixed fourth derivative couples diagonal neighbors and is computed with a nine-point stencil:

$$\left.\frac{\partial^4 w}{\partial x^2 \partial y^2}\right|_{i,j} \approx \frac{1}{h^4}\Big(w_{i+1,j+1} - 2w_{i+1,j} + w_{i+1,j-1} - 2w_{i,j+1} + 4w_{i,j} - 2w_{i,j-1} + w_{i-1,j+1} - 2w_{i-1,j} + w_{i-1,j-1}\Big). \tag{14}$$

Combining the Biharmonic components yields the complete 13-point stencil. In stencil form:

$$\nabla^4 \approx \frac{1}{h^4}\begin{pmatrix} & & 1 & & \\ & 2 & -8 & 2 & \\ 1 & -8 & 20 & -8 & 1 \\ & 2 & -8 & 2 & \\ & & 1 & & \end{pmatrix} \tag{15}$$

Position	Offset (di, dj)	Coefficient
Center	$(0, 0)$	+20
Adjacent	$(\pm1, 0)$, $(0, \pm1)$	−8
Far	$(\pm2, 0)$, $(0, \pm2)$	+1
Diagonal	$(\pm1, \pm1)$	+2

Table 4 Stencil table with ghost points.

From table (4), when the stencil reaches ghost points, the ghost-point mirror relations are substituted. If the mirror point equals the current point, its coefficient is added to the center coefficient. For example, at $(2, 2)$ the stencil requires $w_{0,2}$ and $w_{2,0}$; both mirror to $w_{2,2}$, so the effective center coefficient becomes $20 + 1 + 1 = 22$.

5. Matrix Assembly and example

After spatial discretization, the governing plate equation reduces to a system of second-order ODEs.

$$M\ddot{\mathbf{w}} + C\dot{\mathbf{w}} + K\mathbf{w} = \mathbf{F}(t), \tag{16}$$

where M is the mass matrix, defined as $M = \rho h \cdot I$. C is the damping matrix, defined as $C = K_1 \cdot I$. K is the stiffness matrix, defined as $K = K_0 I - \frac{T}{h^2} L_2 + \frac{D}{h^4} L_4$.

An example of using the discretizing system is when n = 5. At n = 5, the grid indices are $i, j = 1, 2, \ldots, 6$. The boundary corresponds to $i = 1$, $i = 6$, $j = 1$, and $j = 6$, and the interior indices used for solving the PDE are $i, j \in \{2, 3, 4, 5\}$. This yields $(5-1)^2 = 16$, which is the number of unknown interior points. As a result, the discrete operators and the matrices M, C, and K are of size 16×16. This can be mapped, as seen in table (5):

	$i = 2$	$i = 3$	$i = 4$	$i = 5$
$j = 5$	12	13	14	15
$j = 4$	8	9	10	11
$j = 3$	4	5	6	7
$j = 2$	0	1	2	3

Table 5 Values for $n = 5$.

At n = 5, the ghost points relations will be as follows:

$$\begin{aligned} \text{Left:} &\quad w_{0,j} = w_{2,j} \\ \text{Right:} &\quad w_{7,j} = w_{5,j} \\ \text{Bottom:} &\quad w_{i,0} = w_{i,2} \\ \text{Top:} &\quad w_{i,7} = w_{i,5} \end{aligned}$$

Since $M = \rho h \cdot I$ and $C = K_1 \cdot I$, I will be a 16x16 identity matrix due to the 16 interior unknowns:

$$I = \begin{pmatrix} 1&0&0&0&0&0&0&0&0&0&0&0&0&0&0&0 \\ 0&1&0&0&0&0&0&0&0&0&0&0&0&0&0&0 \\ 0&0&1&0&0&0&0&0&0&0&0&0&0&0&0&0 \\ 0&0&0&1&0&0&0&0&0&0&0&0&0&0&0&0 \\ 0&0&0&0&1&0&0&0&0&0&0&0&0&0&0&0 \\ 0&0&0&0&0&1&0&0&0&0&0&0&0&0&0&0 \\ 0&0&0&0&0&0&1&0&0&0&0&0&0&0&0&0 \\ 0&0&0&0&0&0&0&1&0&0&0&0&0&0&0&0 \\ 0&0&0&0&0&0&0&0&1&0&0&0&0&0&0&0 \\ 0&0&0&0&0&0&0&0&0&1&0&0&0&0&0&0 \\ 0&0&0&0&0&0&0&0&0&0&1&0&0&0&0&0 \\ 0&0&0&0&0&0&0&0&0&0&0&1&0&0&0&0 \\ 0&0&0&0&0&0&0&0&0&0&0&0&1&0&0&0 \\ 0&0&0&0&0&0&0&0&0&0&0&0&0&1&0&0 \\ 0&0&0&0&0&0&0&0&0&0&0&0&0&0&1&0 \\ 0&0&0&0&0&0&0&0&0&0&0&0&0&0&0&1 \end{pmatrix}. \tag{17}$$

The Laplacian matrix L_2 is the 5-point stencil assembled from the grid indices i, j. We multiply by $\frac{1}{h^2}$ to obtain the discrete Laplacian operator:

$$L_2 = \begin{pmatrix} -4&1&0&0&1&0&0&0&0&0&0&0&0&0&0&0 \\ 1&-4&1&0&0&1&0&0&0&0&0&0&0&0&0&0 \\ 0&1&-4&1&0&0&1&0&0&0&0&0&0&0&0&0 \\ 0&0&1&-4&0&0&0&1&0&0&0&0&0&0&0&0 \\ 1&0&0&0&-4&1&0&0&1&0&0&0&0&0&0&0 \\ 0&1&0&0&1&-4&1&0&0&1&0&0&0&0&0&0 \\ 0&0&1&0&0&1&-4&1&0&0&1&0&0&0&0&0 \\ 0&0&0&1&0&0&1&-4&0&0&0&1&0&0&0&0 \\ 0&0&0&0&1&0&0&0&-4&1&0&0&1&0&0&0 \\ 0&0&0&0&0&1&0&0&1&-4&1&0&0&1&0&0 \\ 0&0&0&0&0&0&1&0&0&1&-4&1&0&0&1&0 \\ 0&0&0&0&0&0&0&1&0&0&1&-4&0&0&0&1 \\ 0&0&0&0&0&0&0&0&1&0&0&0&-4&1&0&0 \\ 0&0&0&0&0&0&0&0&0&1&0&0&1&-4&1&0 \\ 0&0&0&0&0&0&0&0&0&0&1&0&0&1&-4&1 \\ 0&0&0&0&0&0&0&0&0&0&0&1&0&0&1&-4 \end{pmatrix}. \tag{18}$$

The Biharmonic Matrix L_4 is the 13-point biharmonic stencil assembled on the same grid using the ghost-point mirror relations. We multiply by $\frac{1}{h^4}$ to obtain the discrete biharmonic operator:

$$L_4 = \begin{pmatrix} 22 & -8 & 1 & 0 & -8 & 2 & 0 & 0 & 1 & 0 & 0 & 0 & 0 & 0 & 0 & 0 \\ -8 & 21 & -8 & 1 & 2 & -8 & 2 & 0 & 0 & 1 & 0 & 0 & 0 & 0 & 0 & 0 \\ 1 & -8 & 21 & -8 & 0 & 2 & -8 & 2 & 0 & 0 & 1 & 0 & 0 & 0 & 0 & 0 \\ 0 & 1 & -8 & 22 & 0 & 0 & 2 & -8 & 0 & 0 & 0 & 1 & 0 & 0 & 0 & 0 \\ -8 & 2 & 0 & 0 & 21 & -8 & 1 & 0 & -8 & 2 & 0 & 0 & 1 & 0 & 0 & 0 \\ 2 & -8 & 2 & 0 & -8 & 20 & -8 & 1 & 2 & -8 & 2 & 0 & 0 & 1 & 0 & 0 \\ 0 & 2 & -8 & 2 & 1 & -8 & 20 & -8 & 0 & 2 & -8 & 2 & 0 & 0 & 1 & 0 \\ 0 & 0 & 2 & -8 & 0 & 1 & -8 & 21 & 0 & 0 & 2 & -8 & 0 & 0 & 0 & 1 \\ 1 & 0 & 0 & 0 & -8 & 2 & 0 & 0 & 21 & -8 & 1 & 0 & -8 & 2 & 0 & 0 \\ 0 & 1 & 0 & 0 & 2 & -8 & 2 & 0 & -8 & 20 & -8 & 1 & 2 & -8 & 2 & 0 \\ 0 & 0 & 1 & 0 & 0 & 2 & -8 & 2 & 1 & -8 & 20 & -8 & 0 & 2 & -8 & 2 \\ 0 & 0 & 0 & 1 & 0 & 0 & 2 & -8 & 0 & 1 & -8 & 21 & 0 & 0 & 2 & -8 \\ 0 & 0 & 0 & 0 & 1 & 0 & 0 & 0 & -8 & 2 & 0 & 0 & 22 & -8 & 1 & 0 \\ 0 & 0 & 0 & 0 & 0 & 1 & 0 & 0 & 2 & -8 & 2 & 0 & -8 & 21 & -8 & 1 \\ 0 & 0 & 0 & 0 & 0 & 0 & 1 & 0 & 0 & 2 & -8 & 2 & 1 & -8 & 21 & -8 \\ 0 & 0 & 0 & 0 & 0 & 0 & 0 & 1 & 0 & 0 & 2 & -8 & 0 & 1 & -8 & 22 \end{pmatrix}. \tag{19}$$

Table (6) list each i, j for n = 5 and shows the effective center coefficient used in L_4:

Point (i, j)	Index k	Center	Ghost Point Corrections
$(2, 2)$	0	22	$w_{0,2} = w_{2,2}$ $w_{2,0} = w_{2,2}$
$(3, 2)$	1	21	$w_{3,0} = w_{3,2}$
$(4, 2)$	2	21	$w_{4,0} = w_{4,2}$
$(5, 2)$	3	22	$w_{7,2} = w_{5,2}$ $w_{5,0} = w_{5,2}$
$(2, 3)$	4	21	$w_{0,3} = w_{2,3}$
$(3, 3)$	5	20	None (true interior)
$(4, 3)$	6	20	None (true interior)
$(5, 3)$	7	21	$w_{7,3} = w_{5,3}$
$(2, 4)$	8	21	$w_{0,4} = w_{2,4}$
$(3, 4)$	9	20	None (true interior)
$(4, 4)$	10	20	None (true interior)
$(5, 4)$	11	21	$w_{7,4} = w_{5,4}$
$(2, 5)$	12	22	$w_{0,5} = w_{2,5}$ $w_{2,7} = w_{2,5}$
$(3, 5)$	13	21	$w_{3,7} = w_{3,5}$
$(4, 5)$	14	21	$w_{4,7} = w_{4,5}$
$(5, 5)$	15	22	$w_{7,5} = w_{5,5}$ $w_{5,7} = w_{5,5}$

Table 6 Grid indices and effective coefficients used in L_4 at $n = 5$.

B. Temporal Discretization using the Trapezoidal Method

The Trapezoidal Method was selected due to its second-order accuracy and applicability to vibratory systems such as the plate system we are analyzing. Discretizing the Kirchhoff–Love governing equation leads to a stiff system of ordinary differential equations, where some vibration modes are very fast, while others are very slow, due to the fourth-order derivatives. The Trapezoidal Method is A stable, which ensures numerical stability regardless of the time step size, while it conserves energy well for linear vibration problems and avoids excessive numerical damping that can happen with first-order methods. Thus, the Trapezoidal method is very practical for studying vibration response and impact effects on aircraft skin panels.

The Trapezoidal Method is found by applying the Trapezoid Rule to integrate the velocity and acceleration over the time step $\Delta t = t_{k+1} - t_k$.

1. Derivation for the Simple IVP ($\dot{u} = f(u, t)$)

Starting with the first-order IVP:

$$\dot{u} = f(u, t) \tag{20}$$

$$u(t_0) = u_0 \tag{21}$$

We first integrate the ODE over the interval $[t_k, t_{k+1}]$, which gives:

$$u(t_{k+1}) = u(t_k) + \int_{t_k}^{t_{k+1}} f(u(t), t)dt \tag{22}$$

Approximating with the Trapezoid Rule, which averages the function values at the endpoints:

$$\int_{t_k}^{t_{k+1}} f(u(t), t)dt \approx \frac{\Delta t}{2} \left[f(u_k, t_k) + f(u_{k+1}, t_{k+1}) \right] \tag{23}$$

Once the approximation is substituted back, the implicit Trapezoidal Method is obtained:

$$u_{k+1} = u_k + \frac{\Delta t}{2} \left[f(u_k, t_k) + f(u_{k+1}, t_{k+1}) \right] \tag{24}$$

2. Temporal Truncation Error Analysis

The local truncation error τ_k measures the error introduced in an individual step:

$$\tau_k = \frac{u(t_{k+1}) - u_k}{\Delta t} - \frac{1}{2} \left[f(u_k, t_k) + f(u(t_{k+1}), t_{k+1}) \right]. \tag{25}$$

Using Taylor series expansions of the exact solution $u(t_{k+1})$ and its derivative around t_k gives:

$$u(t_{k+1}) = u_k + \Delta t \dot{u}_k + \frac{\Delta t^2}{2} \ddot{u}_k + \frac{\Delta t^3}{6} \dddot{u}_k + O(\Delta t^4) \tag{26}$$

$$\dot{u}(t_{k+1}) = \dot{u}_k + \Delta t \ddot{u}_k + \frac{\Delta t^2}{2} \dddot{u}_k + O(\Delta t^3) \tag{27}$$

Substituting this Taylor series expansion into the error formula gives us:

$$\tau_k = \frac{1}{\Delta t} \left[\left(u_k + \Delta t \dot{u}_k + \frac{\Delta t^2}{2} \ddot{u}_k + \frac{\Delta t^3}{6} \dddot{u}_k \right) - u_k \right] - \frac{1}{2} \left[\dot{u}_k + \left(\dot{u}_k + \Delta t \ddot{u}_k + \frac{\Delta t^2}{2} \dddot{u}_k \right) \right] + O(\Delta t^3) \tag{28}$$

$$\tau_k = \left[\dot{u}_k + \frac{\Delta t}{2} \ddot{u}_k + \frac{\Delta t^2}{6} \dddot{u}_k \right] - \left[\dot{u}_k + \frac{\Delta t}{2} \ddot{u}_k + \frac{\Delta t^2}{4} \dddot{u}_k \right] + O(\Delta t^3) \tag{29}$$

$$\tau_k = -\frac{1}{12} \Delta t^2 \dddot{u}_k + O(\Delta t^3) \tag{30}$$

The local truncation error scales as $O(\Delta t^3)$, which means that the global error scales as $O(\Delta t^2)$. Therefore, it can be seen that the Trapezoidal Method is second-order accurate.

3. Stability of the Trapezoidal Method

We start by defining the linear stability test equation:

$$\dot{u} = \lambda u, \tag{31}$$

where the amplification factor of the Trapezoidal Method is:

$$R(z) = \frac{1 + z/2}{1 - z/2}, \quad z = \lambda \Delta t. \tag{32}$$

The method is stable whenever $|R(z)| \leq 1$. Fig. (1) shows the stability region of the Trapezoidal Method in the complex z-plane. The entire left half-plane, $\mathrm{Re}(z) \leq 0$, lies within the stability region, showing how the Trapezoidal Method is A-stable. As mentioned earlier, this property is important for stiff systems as it allows large time steps without creating numerical instability.

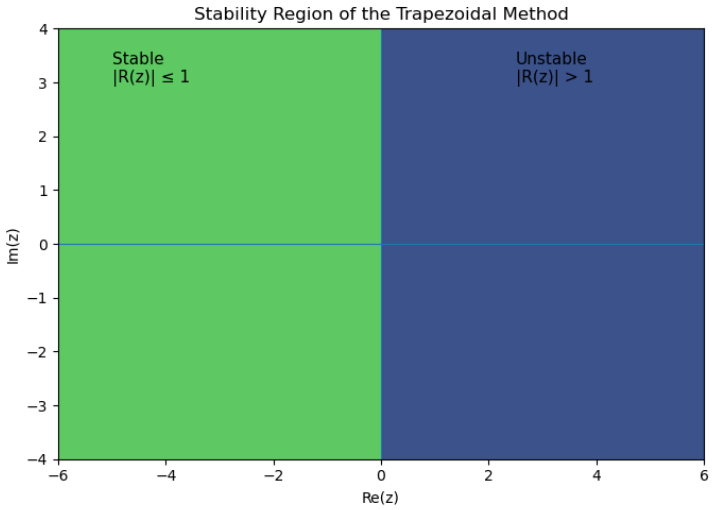

Fig. 1 Stability region of the Trapezoidal Method. The shaded region corresponds to values of $z = \lambda\Delta t$ for which $|R(z)| \leq 1$. The entire left half-plane is stable, demonstrating A-stability.

4. Applications

The Trapezoidal Method corresponds is a form of the Newmark-beta integration method with parameters $\gamma = 1/2$ and $\beta = 1/4$. The Newmark–β method is effectively used in [3] for time integration of a similar system, demonstrating that the Trapezoidal Method is valid for the plate dynamics considered in our system. The integration relations for the second-order system are as follows:

$$\dot{u}_{k+1} = \dot{u}_k + \frac{\Delta t}{2}(\ddot{u}_k + \ddot{u}_{k+1}) \tag{33}$$

$$u_{k+1} = u_k + \Delta t\dot{u}_k + \frac{\Delta t^2}{4}(\ddot{u}_k + \ddot{u}_{k+1}) \tag{34}$$

Applying spatial discretization to the Kirchhoff–Love plate equation using finite differences over the domain Ω gives a system of second-order ODEs that follow the form:

$$M\ddot{w}(t) + C\dot{w}(t) + Kw(t) = f(t), \tag{35}$$

where $w(t)$ is a vector of the out-of-plate nodal displacements, M is the mass matrix, C is the damping matrix, K is the stiffness matrix, and $f(t)$ is the external forces vector.

The stiffness matrix K accounts for plate bending, linear elastic foundation stiffness, and membrane tension, while the damping matrix C represents uniform viscous damping. When assuming linear elasticity and small deflections, the matrices are all constant in time.

5. Time Integration of the System

To advance the solution of Eq. (35) in time, the Trapezoidal Method is applied using the Newmark–beta methodology with parameters $\gamma = \frac{1}{2}$ and $\beta = \frac{1}{4}$, which are equivalent to the implicit trapezoidal rule for first-order systems. The relations for velocity and displacement are:

$$\dot{\mathbf{w}}_{k+1} = \dot{\mathbf{w}}_k + \frac{\Delta t}{2}\left(\ddot{\mathbf{w}}_k + \ddot{\mathbf{w}}_{k+1}\right), \tag{36}$$

$$\mathbf{w}_{k+1} = \mathbf{w}_k + \Delta t\dot{\mathbf{w}}_k + \frac{\Delta t^2}{4}\left(\ddot{\mathbf{w}}_k + \ddot{\mathbf{w}}_{k+1}\right). \tag{37}$$

Substituting these expressions into the equation of motion at time t_{k+1} gives the system:

$$\left(\mathbf{M} + \frac{\Delta t}{2}\mathbf{C} + \frac{\Delta t^2}{4}\mathbf{K}\right)\ddot{\mathbf{w}}_{k+1} = \mathbf{f}_{k+1} - \mathbf{C}\mathbf{v}^* - \mathbf{K}\mathbf{w}^*, \tag{38}$$

where the velocity and displacement estimates are

$$\mathbf{v}^* = \dot{\mathbf{w}}_k + \frac{\Delta t}{2}\ddot{\mathbf{w}}_k, \tag{39}$$

$$\mathbf{w}^* = \mathbf{w}_k + \Delta t\dot{\mathbf{w}}_k + \frac{\Delta t^2}{4}\ddot{\mathbf{w}}_k. \tag{40}$$

Eq. (38) is used to find the acceleration vector $\ddot{w}_{k+1}$ at each time step. The velocity and displacement are then updated using equations (36) and (37).

C. Spatial Truncation Error Analysis

Since the numerical solution involves spatial and temporal discretization, accuracy must be found for both space and time domains. We demonstrate that the finite difference discretization of the Kirchhoff–Love plate equation has a spatial truncation error of $O(\Delta x^2)$.

The spatial operators requiring discretization are the Laplacian $\nabla^2 w$ and biharmonic $\nabla^4 w$.

1. Truncation Error for the Laplacian

The Laplacian is discretized using the central difference formula:

$$\left.\frac{\partial^2 w}{\partial x^2}\right|_i \approx \frac{w_{i+1} - 2w_i + w_{i-1}}{\Delta x^2}. \tag{41}$$

Expanding w_{i+1} and w_{i-1} in Taylor series about point i gives:

$$w_{i+1} = w_i + \Delta x\frac{\partial w}{\partial x} + \frac{\Delta x^2}{2}\frac{\partial^2 w}{\partial x^2} + \frac{\Delta x^3}{6}\frac{\partial^3 w}{\partial x^3} + \frac{\Delta x^4}{24}\frac{\partial^4 w}{\partial x^4} + O(\Delta x^5), \tag{42}$$

$$w_{i-1} = w_i - \Delta x\frac{\partial w}{\partial x} + \frac{\Delta x^2}{2}\frac{\partial^2 w}{\partial x^2} - \frac{\Delta x^3}{6}\frac{\partial^3 w}{\partial x^3} + \frac{\Delta x^4}{24}\frac{\partial^4 w}{\partial x^4} + O(\Delta x^5). \tag{43}$$

Adding these expressions together results in:

$$w_{i+1} + w_{i-1} = 2w_i + \Delta x^2\frac{\partial^2 w}{\partial x^2} + \frac{\Delta x^4}{12}\frac{\partial^4 w}{\partial x^4} + O(\Delta x^6). \tag{44}$$

Note that the odd-power terms cancel due to the symmetry of the central difference stencil. Rearranging gives:

$$\frac{w_{i+1} - 2w_i + w_{i-1}}{\Delta x^2} = \frac{\partial^2 w}{\partial x^2} + \frac{\Delta x^2}{12}\frac{\partial^4 w}{\partial x^4} + O(\Delta x^4). \tag{45}$$

Therefore, the truncation error for the second derivative is:

$$\boxed{\tau_{\nabla^2} = O(\Delta x^2)}. \tag{46}$$

The same analysis applies to $\partial^2 w/\partial y^2$, giving $O(\Delta y^2)$.

2. Truncation Error for the Biharmonic

The fourth derivative is discretized as:

$$\left.\frac{\partial^4 w}{\partial x^4}\right|_i \approx \frac{w_{i+2} - 4w_{i+1} + 6w_i - 4w_{i-1} + w_{i-2}}{\Delta x^4}, \tag{47}$$

which is expanding all terms in Taylor series. Let $w' = \partial w/\partial x$, $w'' = \partial^2 w/\partial x^2$, etc. Then:

$$w_{i\pm1} = w_i \pm \Delta x w' + \frac{\Delta x^2}{2} w'' \pm \frac{\Delta x^3}{6} w''' + \frac{\Delta x^4}{24} w^{(4)} \pm \frac{\Delta x^5}{120} w^{(5)} + \frac{\Delta x^6}{720} w^{(6)} + O(\Delta x^7), \tag{48}$$

$$w_{i\pm2} = w_i \pm 2\Delta x w' + 2\Delta x^2 w'' \pm \frac{4\Delta x^3}{3} w''' + \frac{2\Delta x^4}{3} w^{(4)} \pm \frac{4\Delta x^5}{15} w^{(5)} + \frac{4\Delta x^6}{45} w^{(6)} + O(\Delta x^7). \tag{49}$$

Computing the linear combination $w_{i+2} - 4w_{i+1} + 6w_i - 4w_{i-1} + w_{i-2}$, table (7) shows the coefficients of each derivative term:

Term	Coefficient
w_i	$1 - 4 + 6 - 4 + 1 = 0$
$\Delta x\, w'$	$2 - 4 + 0 + 4 - 2 = 0$
$\Delta x^2 w''$	$2 - 2 + 0 - 2 + 2 = 0$
$\Delta x^3 w'''$	$\frac{4}{3} - \frac{2}{3} + 0 + \frac{2}{3} - \frac{4}{3} = 0$
$\Delta x^4 w^{(4)}$	$\frac{2}{3} - \frac{1}{6} + 0 - \frac{1}{6} + \frac{2}{3} = 1$
$\Delta x^5 w^{(5)}$	$\frac{4}{15} - \frac{1}{30} + 0 + \frac{1}{30} - \frac{4}{15} = 0$
$\Delta x^6 w^{(6)}$	$\frac{4}{45} - \frac{1}{180} + 0 - \frac{1}{180} + \frac{4}{45} = \frac{1}{6}$

Table 7 Coefficients for each derivative in the biharmonic expansion.

This yields:

$$w_{i+2} - 4w_{i+1} + 6w_i - 4w_{i-1} + w_{i-2} = \Delta x^4 w^{(4)} + \frac{\Delta x^6}{6} w^{(6)} + O(\Delta x^8), \tag{50}$$

Dividing by Δx^4 gives:

$$\frac{w_{i+2} - 4w_{i+1} + 6w_i - 4w_{i-1} + w_{i-2}}{\Delta x^4} = \frac{\partial^4 w}{\partial x^4} + \frac{\Delta x^2}{6} \frac{\partial^6 w}{\partial x^6} + O(\Delta x^4). \tag{51}$$

Therefore, the truncation error for the fourth derivative is:

$$\boxed{\tau_{\partial^4/\partial x^4} = O(\Delta x^2)}. \tag{52}$$

3. Mixed Derivative

The mixed derivative $\partial^4 w/\partial x^2 \partial y^2$ is computed by applying the second derivative stencil in x and then in y:

$$\left.\frac{\partial^4 w}{\partial x^2 \partial y^2}\right|_{i,j} \approx \frac{1}{\Delta x^2 \Delta y^2} \Big(w_{i+1,j+1} - 2w_{i+1,j} + w_{i+1,j-1} - 2w_{i,j+1} + 4w_{i,j} - 2w_{i,j-1} + w_{i-1,j+1} - 2w_{i-1,j} + w_{i-1,j-1} \Big). \tag{53}$$

Since each second derivative operator has $O(\Delta x^2)$ or $O(\Delta y^2)$ error, the mixed derivative has:

$$\boxed{\tau_{\partial^4/\partial x^2 \partial y^2} = O(\Delta x^2) + O(\Delta y^2)}. \tag{54}$$

4. Total Spatial Truncation Error

The full biharmonic operator is:

$$\nabla^4 w = \frac{\partial^4 w}{\partial x^4} + 2\frac{\partial^4 w}{\partial x^2 \partial y^2} + \frac{\partial^4 w}{\partial y^4}. \tag{55}$$

Table (8) combines the truncation errors of all spatial operators in the plate equation. Eq. (56) is the total spatial truncation error of the discretized plate equation over a uniform grid with $\Delta x = \Delta y = h$:

Operator	Stencil	Truncation Error
$\partial^2 w/\partial x^2$	3-point	$O(\Delta x^2)$
$\partial^2 w/\partial y^2$	3-point	$O(\Delta y^2)$
$\nabla^2 w$	5-point	$O(\Delta x^2) + O(\Delta y^2)$
$\partial^4 w/\partial x^4$	5-point	$O(\Delta x^2)$
$\partial^4 w/\partial y^4$	5-point	$O(\Delta y^2)$
$\partial^4 w/\partial x^2 \partial y^2$	9-point	$O(\Delta x^2) + O(\Delta y^2)$
$\nabla^4 w$	13-point	$O(\Delta x^2) + O(\Delta y^2)$

Table 8 Truncation errors of spatial operators for the plate equation.

$$\boxed{\tau_{\text{spatial}} = O(h^2)}. \tag{56}$$

This second-order spatial accuracy is a direct consequence of using symmetric (central) finite difference stencils, which cause the odd-power terms in the Taylor expansion to cancel.

D. Numerical Method Summary

Having defined the second-order spatial accuracy of the finite difference discretization and the second-order temporal accuracy and stability of the Trapezoidal Method, the step by step solution procedure for the Trapezoidal method can be summarized as follows:

1) Discretize the spatial domain and define the mass matrix **M**, stiffness matrix **K**, and damping matrix **C**.
2) Apply clamped boundary conditions.
3) Initialize displacement w_0 and velocity $\dot{w}_0$ from the given initial conditions.
4) Find initial acceleration $\ddot{w}_0$ from Eq. (35).
5) For each time step $k \rightarrow k + 1$:
    1) Define the system in Eq. (38).
    2) Solve for $\ddot{w}_{k+1}$.
    3) Update velocity and displacement using Eqs. (36)–(37).

The complete numerical implementation code corresponding to this algorithm can be found at `https://github.com/NikosMonogyios/AE370_Group_Project_2/`.

IV. Implementation of the Chosen Method

A. Simulation Parameters Selection

Based on the findings of [4], we chose the parameters F_0, a and b to be 10^4, 6 ms, and 2 ms^2 respectively. To ensure enough time-steps during the period that the impulse is applied, the Δt value was chosen to be 0.05 ms. Additionally, in order to observe the behavior of the plate after the force is applied, the total simulation time span was selected to be 25 ms. In terms of spatial discretizations we chose a value of n = 75, which corresponds to $h \approx 6.667mm$. This choice was made in order to balance the accuracy of the simulations and computational time. Since the spatial discretization matrices are $(n-1)^2\, x\, (n-1)^2$ matrices, the computational resources needed and, hence, the computational time increase quadratically as we increase n. In order to afford such a high n, without the need for hour-long simulations, the code implements LU decomposition for the solution of equation (38). This significantly reduced the simulation time from 0.5-1 hour to a few minutes.

B. Spatial Convergence Study

In order to verify that the total error scales with Δx^2 (or Δy^2 since the grid is uniform), we calculated the percent error at $T = 0.1s$ using Eq. (57):

$$||e|| = \frac{||\mathbf{w_n}(\mathbf{x}, T) - \mathbf{w_{n_{Base}}}(\mathbf{x}, T)||}{||\mathbf{w_{n_{Base}}}(\mathbf{x}, T)||}. \tag{57}$$

For this study, n_{Base} was chosen to be 80 and the error was calculated for n = [10, 20, 30, 40, 50, 60, 75]. The error was the plotted vs Δx, in both cartesian and log-log graphs, which can be seen in Fig. (2). Because of the fact that changing the n changes the size of the $\mathbf{w_n}(\mathbf{x}, T)$, the vector $\mathbf{w_n}(\mathbf{x}, T)$ had to be projected using linear interpolation to another vector $\mathbf{w'_n}(\mathbf{x}, T)$ that had the same size as $\mathbf{w_{n_{Base}}}(\mathbf{x}, T)$. Additionally, the function $f(\Delta x) = s\,\Delta x^2$ was added to the plots. The variable s is a scale factor used in order to make it easier to identify that the global error indeed scales with Δx^2. Since we only want to investigate the effects of the spatial error, a sufficiently small $\Delta t = 0.05$ ms was chosen to minimize the effects of the temporal error. The error plots obtained here also seem to match the error plots from [[3]]

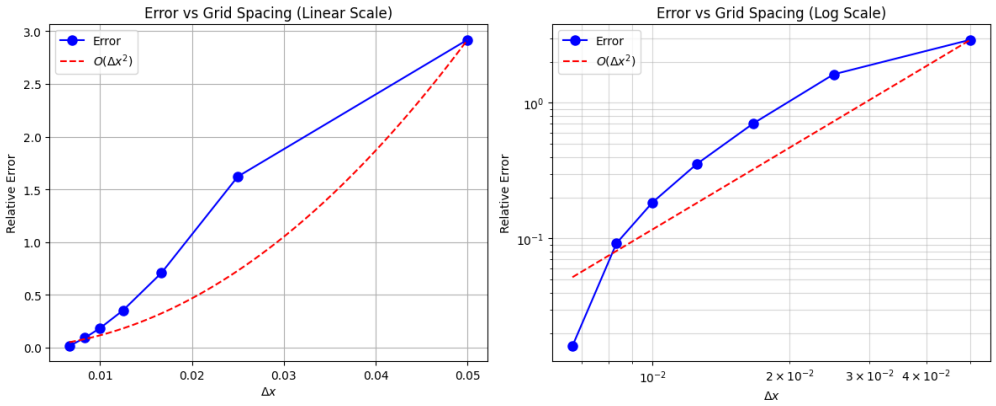

Fig. 2 Global Error vs grid element size Δx

C. Temporal Convergence Study

Similarly to the spatial convergence, a study was conducted to verify that the global error scales with Δt^2. In this case, $\Delta t_{base} = 5\,\mu s$ was used, and the error was calculated for Δt = [0.00001, 0.00002, 0.00005, 0.0001, 0.0002, 0.0005] s. In order to minimize the effect of the spatial error, a sufficiently small n = 50 was used. Finally, since n = constant, all of the $\mathbf{w_n}(\mathbf{x}, T)$ have the same length, and therefore, no interpolation of the results is needed. The convergence plot for the temporal convergence study can be found in Fig. (3). It can now be verified that the global error scales with Δt^2

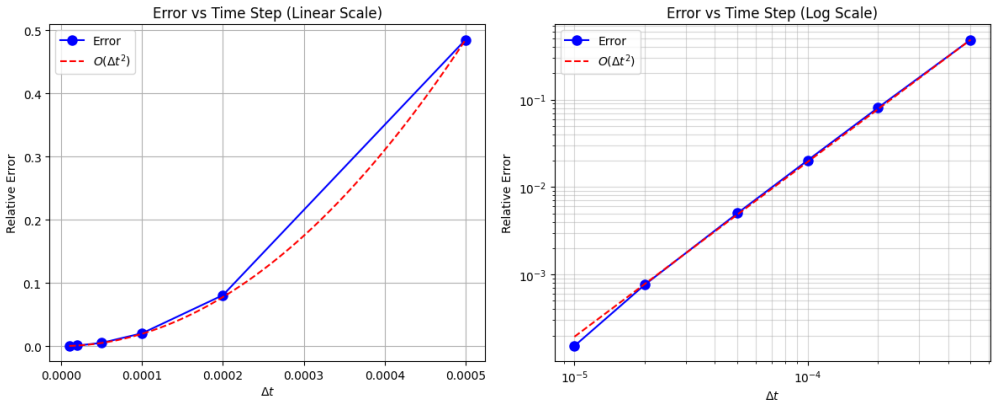

Fig. 3 Global Error vs time-step size Δt

V. Results

Before we begin to explore the results, we first need to discuss what we measured and why. The main outputs we sought were the distribution and magnitude of displacement and the stresses (σ_x,σ_y, τ) over time. We chose these variables to measure, as too much deformation/stress will lead to a failure occurring, so seeing where and to what magnitude they occur is important to prevent failure. Then, also by seeing it over time, we can see if vibrations will be an issue we should take into account to prevent failure from fatigue.

To start, let's look at the impact force made by the forcing function and the displacement at the center of each of the plates over time. Looking at Figs. (4), (5) and (6), we see that all of them experience the same impact force, and then all of the panels experience displacement vibrations. This shows us immediately that vibrations are caused by impacts, and so failures due to fatigue should be taken into account. Taking a closer look, we can see they all do have slight variations, with the most obvious being the amount of maximum displacement each of the experiences has. We can see that the aluminum experiences the most with about 0.015 m of max displacement, then titanium with about 0.01 m of max displacement, and finally with the least stainless steel at 0.006 m of max displacement. These results are expected as they are proportional to the Young's Modulus of each material. It shows us that steel is clearly the best choice for materials for places that experience high impact forces. More interestingly, we can look at the frequency of the vibrations. Although we did not exactly measure frequency, we can look at how far past the 7th positive peak each material's vibrations occurred to compare the frequencies to each other. From this, we can see that titanium had the highest frequency, then aluminum, and steel with the lowest. This means that steel is the best for places that experience many impacts, as with a lower frequency, it will go through fewer displacement cycles. That is, without even taking into account steel's inherent resistance to fatigue failures. Although steel is the best material at resisting impacts, it is so heavy that, at most, you can use it only for high-impact areas. But even then, with being almost half the density but experiencing less than half the amount of displacement, titanium is still likely a better choice.

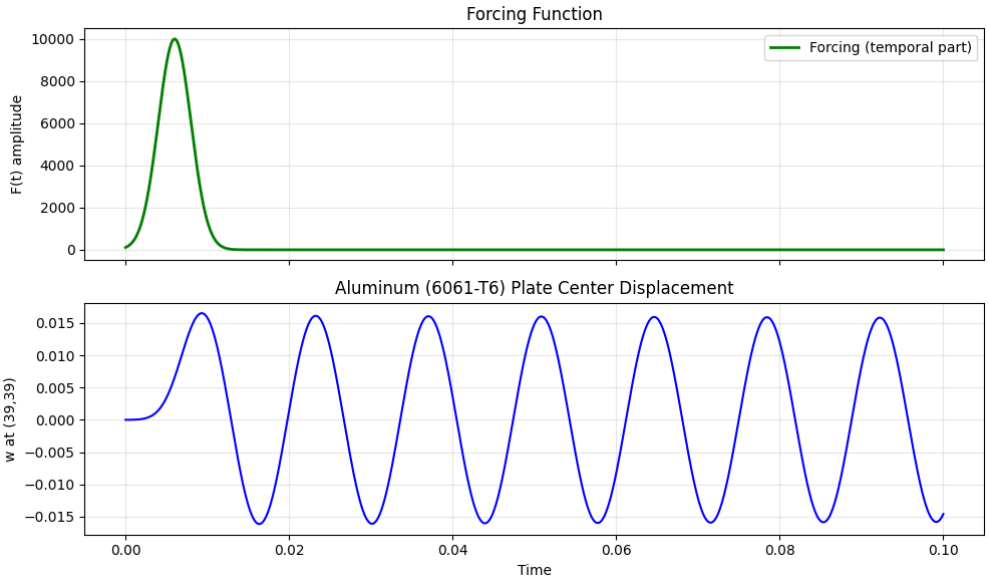

Fig. 4 Forcing function and Aluminum plate center displacement over time.

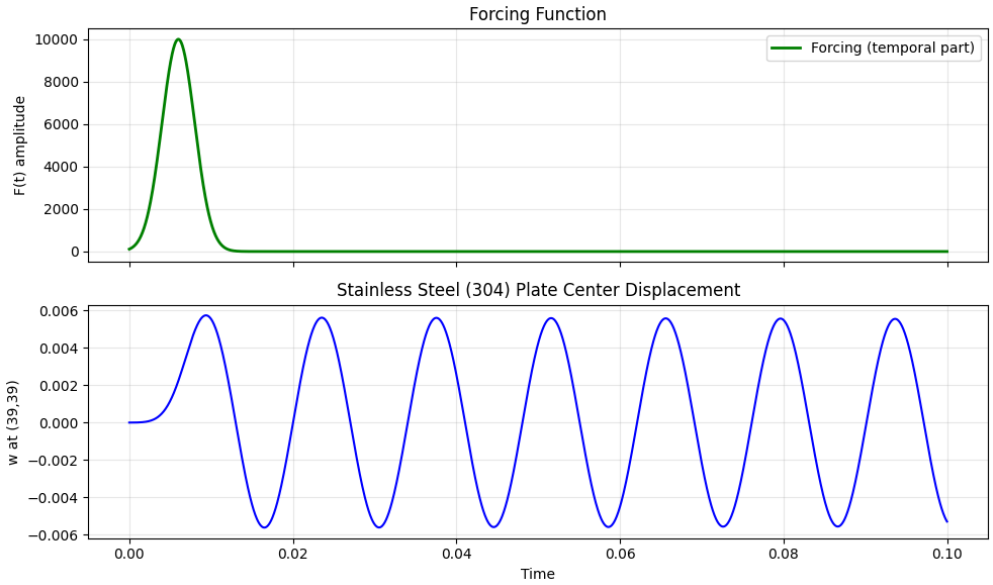

Fig. 5 Forcing function and Stainless Steel plate center displacement over time.

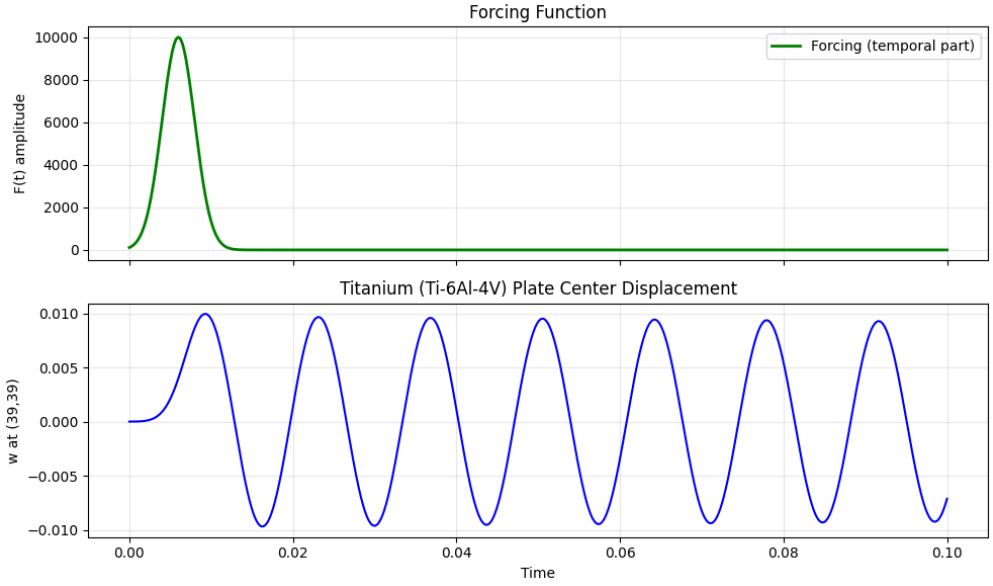

Fig. 6 Forcing function and Titanium plate center displacement over time.

Next, we want to look at the displacement distribution over time. We can see in Figs. (7), (8) and (9) that nearly all of the displacement is concentrated at the center of the plate where the impacts occur, and over time, it cycles between positive and negative displacement. We can also see that between the different materials, they all follow this exact same behavior with just slightly different times and magnitudes, just like how was shown for the center displacements. This distribution of displacement is completely expected as the center is experiencing the impact it is experiencing the highest forces with the least amount of support, making it so it experiences the highest displacement of any region. From this, it is very clear that when a large impact happens at the point of the impact, there should be an inspection to ensure that there is no permanent deformation caused.

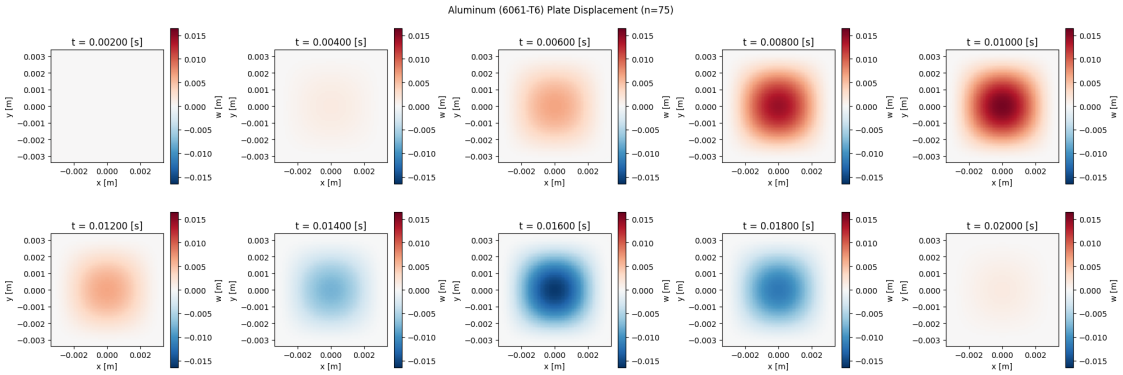

Fig. 7 Aluminum plate distribution of displacement over time.

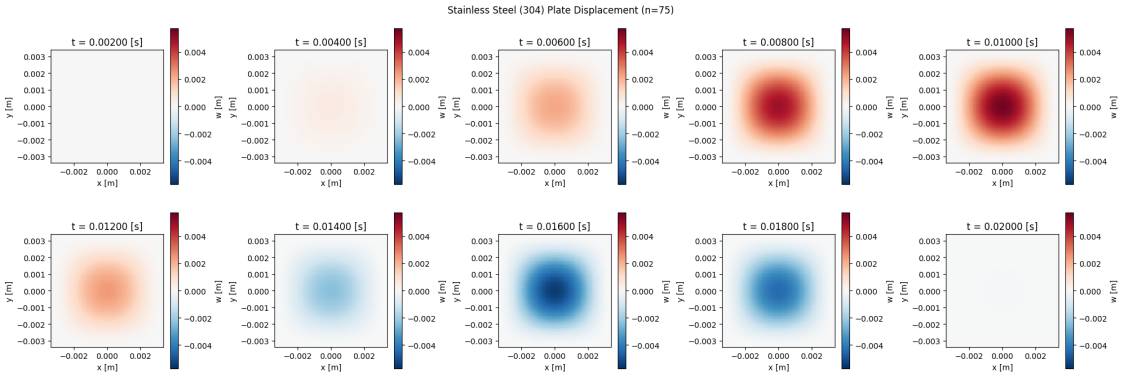

Fig. 8 Stainless Steel plate distribution of displacement over time.

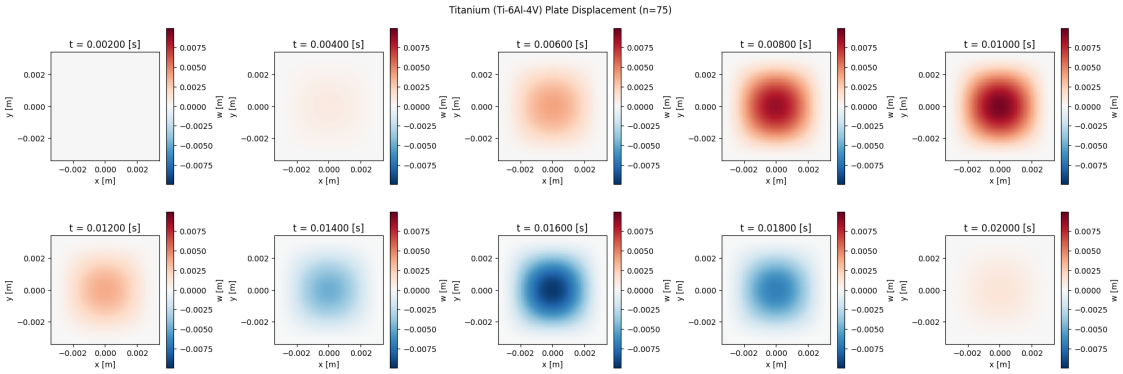

Fig. 9 Titanium plate distribution of displacement over time.

Finally, we want to look at the stress distributions over time for the plates. For all of the materials, the stress distributions look very similar, with the only differences being the same, with the displacement distributions being the magnitudes and slight timing differences from the different frequencies. Because of that, we will just be looking at the stresses on the aluminum plates, as they are most commonly used as a panel. Firstly, looking at Figs. (10) and (11), we can see an expected normal stress distribution with stresses at the middle of the plate and the highest stresses at the plate boundaries being at about 150MPa. We can also see how the stresses gradually flip signs, showing the vibrations. Next, looking at the shear stresses in Fig. (12), we get a stress distribution which at first, is less intuitive as it makes a checkerboard pattern slightly offset from the walls, with at most about 30MPa. But when comparing it to the normal

stress distribution, we can see the shear stress maxes are between the areas of max σ_x, and σ_y, leading to shear stress. Applying these stress maps to the real world is very useful, as it can help us know where we can expect failures. With the highest forces being at the boundaries, it is very clear that those areas should be inspected the most to ensure there are no failures. The middle should also be inspected, but since it is dealing with lower stresses, it will not need to be as often. Finally, since the corners are experiencing mostly shear stress and it is an order of magnitude less than the normal stresses, they will not need to be inspected as often.

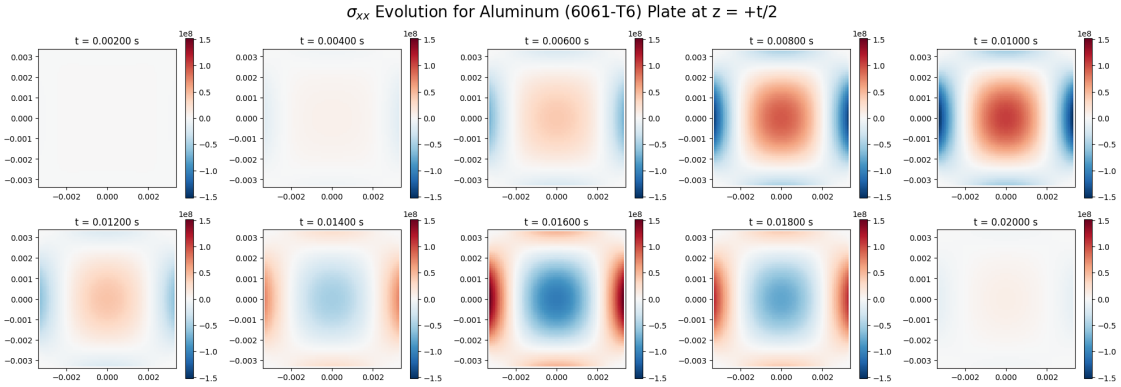

Fig. 10 Distribution of σ_x on a plate over time.

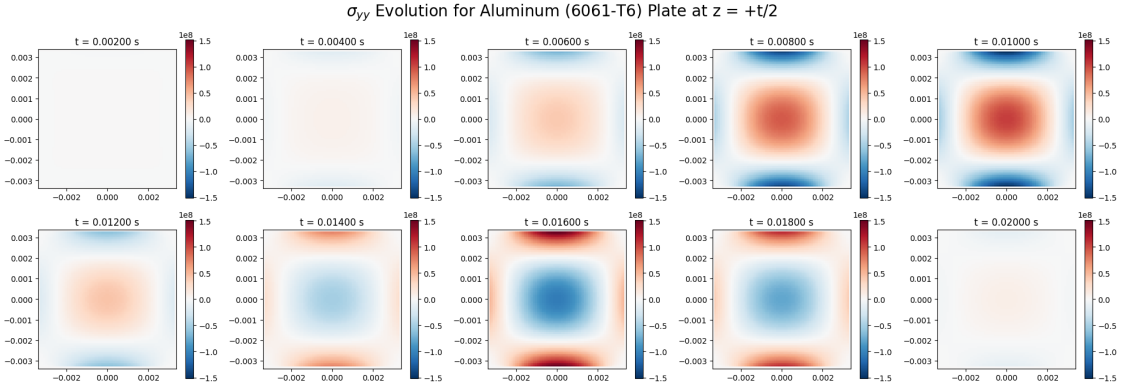

Fig. 11 Distribution of σ_y on a plate over time.

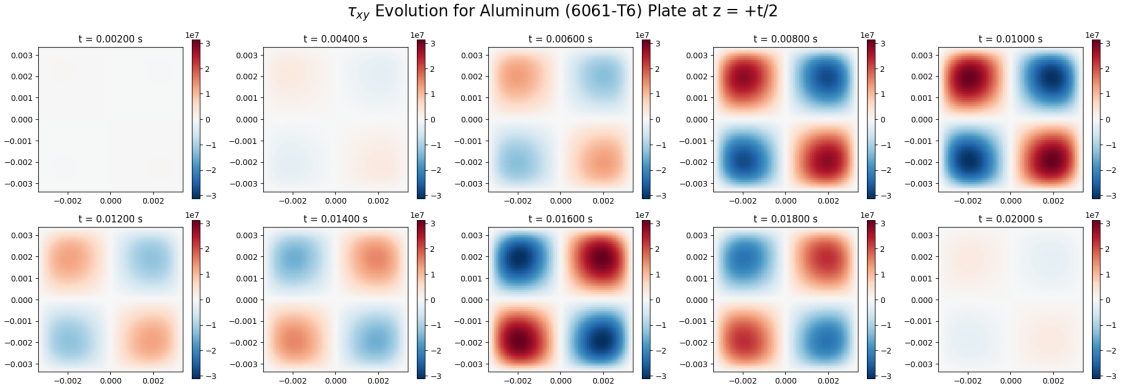

Fig. 12 Distribution of τ on a plate over time.

Team Management Summary

The group consists of four members: Nikolaos Monogyios, Will Brizzolara, Gabriel Esquivel and Ka'inoa Lugo. Our project aimed to model and solve an initial boundary value problem governing the response of a thin aircraft fuselage plate under a distributed impact force. The goal was to evenly divide the work for each member, which was done primarily by designating one group member for each of the four primary sections of the report. The team contributions are as follows:

- $\approx$ 25% – Nikolaos Monogyios: Primarily responsible for the section **Implementation of the Method**. Worked on the derivation of the governing equation, and the spatial discretization equations and truncation error. Created the Python script that solves the equation numerically and plots the results. Additionally, selected modeling parameters and appropriate time-step Δt
- $\approx$ 25% – Will Brizzolara: Primarily responsible for writing the **Results** sections. This section goes over the data from the simulation, why we presented the data in that way and how the data relates and is useful for engineering. Additionally assisted in the initial research focusing on material parameters and equations for material constants.
- $\approx$ 25% – Gabriel Esquivel: Primarily responsible for writing the **Introduction to the Dynamical System** section. The section includes introducing the IBVP, conditions, an example, and the model our team chose. The section targeted three points: why the IBVP is interesting/important to understand, creating questions to test the IBVP, and conveying the IBVP mathematically, with the parameters being set for the project. Additionally set up the document layout, format, and abstract, and assisted in initial research for the mathematical equations.
- $\approx$ 25% – Ka'inoa Lugo: Primarily responsible for writing the **Numerical Approach for the System** section. This involved validating the trapezoidal numerical integration method chosen and the Kirchhoff Love plate model for the system. Also derived the governing equations, formulating the time integration scheme, and presenting the algorithmic summary used for time advancement of the system response. Additionally outlined and contributed to the **Team Management Summary** section.

Acknowledgments

We note that we used AI to assist in writing LaTex code to format more complex equations accurately within the text. We also used AI to assist us in finding relevant, reputable sources that helped us understand methods and modeling for the system we are replicating. Finally, AI was used to modify and troubleshoot code in order to improve efficiency and code quality. Examples of that include the addition of dictionaries for easier reference of variables, functions that enable us to review the progress of the simulation and suggestions on how to fix errors. It is important to note that any part of this report that has been obtained with the help of AI models has been reviewed and verified by members of the team.

References

[1] Liu, X., "Impact response and crashworthy design of composite fuselage structures: An overview," https://www.sciencedirect.com/science/article/pii/S0376042124000289, 2024. [Accessed 9-12-2025].

[2] Jia, S., "Numerical study on the impact response of aircraft fuselage structures subjected to large-size tire fragment," https://pmc.ncbi.nlm.nih.gov/articles/PMC10453686/, 2024. [Accessed 9-12-2025].

[3] NGUYEN, D. T. A., "STABLE AND ACCURATE NUMERICAL METHODS FOR GENERALIZED KIRCHHOFF-LOVE PLATES," https://arxiv.org/pdf/2008.01693, 2022. [Accessed 13-12-2025].

[4] Nizampatnam, L. S., "Finite Element Modelling for Bird Strike Analysis and Review of Existing Numerical Methods," Technical report, Wichita State University, 2018. URL https://soar.wichita.edu/server/api/core/bitstreams/b63e0d48-a5fd-425f-b034-574267ca1582/content.